

The structure of SrTiO₃(001)-2×1 surface analyzed by high-resolution medium energy ion scattering coupled with *ab initio* calculations

Taishi Matsuda, Yuki Yoshida, Kei Mitsuhashi, and Yoshiaki Kido*

Department of Physics, Ritsumeikan University, Kusatsu, Shiga-ken, 525-8577, Japan

Abstract

High-resolution medium energy ion scattering (MEIS) spectrometry coupled with photoelectron spectroscopy revealed unambiguously that the initial SrTiO₃(001) surface chemically etched in a buffered NH₄F-HF solution was perfectly terminated with a single-layer (SL) of TiO₂(001) and annealing the surface at 600 - 800°C in ultrahigh vacuum (UHV) led to a (2×1)-reconstructed surface terminated with a double-layer (DL) of TiO₂(001). After annealing in UHV, rock-salt SrO(001) clusters with two atomic layer height grew epitaxially on the DL-TiO₂(001)-2×1 surface with a coverage of 20-30 %. High-resolution MEIS combined with *ab initio* calculations demonstrated the structure of the DL-TiO₂(001)-2×1 surface close to that proposed by Erdman et al.[Nature **419**, 55 (2002)] and ruled out the structure predicted by Herger et al.[Phys. Rev. Lett. **98**, 076102 (2007)]. Based on the MEIS analysis combined with the *ab initio* calculations, we propose the most probable (2×1) surface structure.

I. INTRODUCTION

Strontium titanate (SrTiO_3 : STO) crystal taking a typical perovskite structure has attracted much attention recently since the finding of two-dimensional (2D) electron gas formed at vacuum-cleaved and H-terminated surfaces[1,2]. Aside from the electronic properties, the structure of the surfaces depends on annealing temperature and changes in a variety of fashion[3-8]. The $\text{SrTiO}_3(001)$ surface consists of alternating stacking of $\text{TiO}_2(001)$ and $\text{SrO}(001)$ planes and it was reported that the (001) surface is terminated perfectly by $\text{TiO}_2(001)$ plane after etching in a pH-controlled buffered $\text{NH}_4\text{F-HF}$ (BHF) solution[9]. According to our previous study, after annealing the surface in ultrahigh vacuum (UHV) the $\text{SrO}(001)$ plane emerged partly[10]. Ohnishi et al.[11] analyzed *in situ* the surfaces of as-supplied samples before and after annealing in UHV by low energy ion scattering and found that the SrO face started to appear at temperatures above 200°C and the areal occupation ratio was saturated at $\sim 12\%$ at 400°C , while the surface re-etched in BHF was terminated perfectly with $\text{TiO}_2(001)$ and stable up to 700°C . Here, the as-supplied sample corresponds to the commercially available BHF-treated substrate with flat steps terminated with $\text{TiO}_2(001)$ face.

Concerning the atomic configurations of the (001) surfaces, Castell[5] reported that annealing the BHF-treated surface at $600 - 800^\circ\text{C}$ led to a $(2 \times 1) + (1 \times 2)$ mixed phase with wide and flat terraces whose step height was 4.0 \AA corresponding to two-atomic layer height. Further annealing the surface at temperatures above 900°C gives a $c(4 \times 4)$ reconstruction. Of course, the above surfaces have oxygen deficiency in the top $\text{TiO}_2(001)$ plane. The (1×1) nearly stoichiometric surface is obtained by annealing around 600°C in O_2 ambient ($\sim 1 \times 10^{-6}$ Torr)[10]. It has been for a long time recognized that the TiO_2 -terminated surface consists of the single layer (SL) of $\text{TiO}_2(001)$. Erdman et al.[6] showed the (2×1) surface terminating not with one, but two TiO_2 atomic layers by transmission electron microscopy (TEM) and proposed a structure model. After that Herger et al.[7,12] analyzed the $\text{SrTiO}_3(001)$ surface where three different terminations of (2×1) , and (2×2) reconstruction as well as a (1×1) relaxation coexisted and extracted all the structures terminated with double-layer (DL) of TiO_2 by surface X-ray diffraction (SXRD) combined with the density functional calculations. However, the above two structure models for the (2×1) surface are quite different. The problem in the above analyses using electron and X-ray diffractions resides in too many fitting parameters, particularly in the latter more than 40 including the fractions of the (1×1) , (2×1) , and (2×2) surfaces, which probably tend to mislead one to an incorrect structure

model. In spite of the above two reports, the fact that the STO(001) surfaces annealed in UHV is terminated with the DL-TiO₂(001) is not yet recognized well.

Previously, we prepared the STO(001)-1×1 surface and determined the ruffled and relaxed surface structure by high-resolution medium energy ion scattering (MEIS) spectroscopy based on the assumption that the surface is terminated with a single-layer (SL) TiO₂[10,13]. In the previous MEIS spectrum analysis, an unresolved question was left that the surface peak coming from the top TiO₂(001) plane was significantly broader than that expected from the SL-TiO₂ termination. This may be puzzled out by assuming the DL-TiO₂ termination. In the present study, first we show the structure change of the STO(001) surface by elevated temperatures from room temperature (RT) up to 800°C in UHV using high-resolution MEIS coupled with photoelectron spectroscopy. It is demonstrated that the single phase STO(001)-2×1 surface emerges at temperatures from 400 up to 800°C and on top of the surface rock-salt SrO clusters grow epitaxially. The observed MEIS spectra for the (2×1) surface, however, could not be reproduced by assuming the two structure models proposed so far based on the TEM[7] and SXRD[12] analyses. It is emphasized that the MEIS analysis is based on the particle nature of medium energy ions and thus atomic structures are determined directly in a real space, quite different from diffractions in a momentum space. We also performed *ab initio* calculations using VASP (Vienna *ab initio* simulation package)[14,15] and propose the most probable surface structure, which is energetically stable and able to reproduce the observed MEIS spectra.

II. EXPERIMENT

The experiment was performed at the beamline 8 named SORIS working at Ritsumeikan Synchrotron-Radiation (SR) Center, where the following three modules are connected each other, (i) sample preparation, (ii) MEIS, and (iii) photoemission analysis systems. This allows basically for *in situ* analyses under ultrahigh vacuum (UHV) conditions ($< 2 \times 10^{-10}$ Torr). Our MEIS system makes it possible to determine the subsurface atomic positions with an accuracy of ~ 0.01 Å[16,17] and the photoemission analysis identifies the clusters segregated on the surface by annealing in UHV.

We purchased the mirror-finished STO(001) substrates treated by pH controlled buffered HF (BHF), whose surfaces were terminated perfectly by TiO₂(001) plane[1], which will be confirmed later by MEIS. Indeed, atomic force microscopy observation under an atmospheric condition showed stepped surfaces with wide and flat terraces

whose step height is 4.0 Å. To be free from electric charging-up, the substrates used were Nb-doped (0.05 wt %) and thus n-type semiconductors. The surfaces were rinsed in acetone by an ultrasonic cleaner and then dipped into a BHF (pH: 4.2) for 10 min before introducing that into a UHV scattering chamber. Annealing the as-supplied samples at 600 and 800°C for 30 min led to a clean surface with a 2×1 reconstruction, which was checked by reflection high energy electron diffraction (RHEED) and Auger electron spectroscopy. The observed RHEED pattern with clear Kikuchi lines was a 2×1 structure not a mixed (2×1) and (1×2) phase, clearly showing preferred ordering along [100] or [010] axis. Valence band spectra observed using SR light showed a gap state about 1 eV below the Fermi level for the 2×1 surface, which originates from O-vacancies created on top of the surface (not shown here). The observed intensity became maximum at a photon energy of ~50 eV, indicating the source coming from Ti 3d electrons provided by surface O vacancies[18]. The Ti 3p electron is resonantly excited at $h\nu = \sim 50$ eV into the 3d state and then decayed via emission of a photoelectron ($\text{Ti } 3p^6 3d^1 + h\nu \rightarrow \text{Ti } [3p^5 3d^2]^* \rightarrow \text{Ti } 3p^6 3d^0 + e^-$). The STO(001)-2×1 surface without the gap state was also formed by annealing the as-supplied substrate at 800°C in an O₂ pressure of 1×10^{-8} Torr for 30 min. Therefore, the STO(001)-2×1 reconstruction is not necessarily induced by creation of O vacancies. The detail of the (2×1) structure correlated with the electronic state is beyond the scope of this work.

The high-resolution MEIS measurement was performed using 120 keV He⁺ ions and the scattered He⁺ ions were detected by a toroidal electrostatic analyzer (ESA) with an energy resolution of 1.0×10^{-3} (full-width at a half maximum: FWHM)[16]. The accelerated He⁺ beam was collimated to 0.18 mm in the horizontal plane and 2.0 mm in the vertical direction before impinging on the sample surface. Such a small size of the incident beam and excellent spatial resolution (40 μm) of the position-sensitive detector connected to the toroidal ESA give the superior energy resolution and thus allow for layer-by-layer analysis. The sample was mounted on a 6-axis goniometer and positively biased at 90 V to the ground to suppress secondary electrons emission, allowing for a precise measurement of the integrated beam current. This is essential to derive absolute amounts of constituent atomic species. In order to avoid radiation damage by He⁺ irradiation, we shifted the beam position slightly after accumulating the beam current of 1 μC.

III. RESULTS AND DISCUSSION

A. Structure Change by Annealing in UHV

Before showing MEIS results, how to analyze a MEIS energy spectrum is explained briefly. The scattering yield from an atomic species j in the n -th atomic-layer is expressed by

$$Y_j(n) = Q (d\sigma/d\Omega)_j \Delta\Omega \cdot (N_j \Delta x) P_{CL}^{(j)}(n) \varepsilon \eta_+ / \cos \theta_m, \quad (1)$$

where Q , $(d\sigma/d\Omega)_j$, $\Delta\Omega$, and $N_j \Delta x$ are number of incident He^+ ions, scattering cross section, solid angle subtended by the toroidal ESA (0.76×10^{-4} str), and number of target atoms (atoms/cm^2), respectively. The detection efficiency, He^+ fraction for scattered He ions, and incident angle with respect to surface normal are denoted by ε (0.44), η_+ , and θ_{in} , respectively. The He^+ fraction (η_+) is dependent on a surface material and emerging energy[19] and thus the η_+ value for He ions emerging from the TiO_2 face was determined in advance using rutile $\text{TiO}_2(110)$ surfaces whose structure was already known[20]. Here, $P_{CL}^j(n)$ corresponds to the close encounter probability for the atoms j in the n -th layer, which is normalized by that for the atoms subjected to no shadowing and blocking effects[21] such as the atoms on top. These effects emerge for single crystal samples consisting of regular arrays of crystal planes and axes. Note that the projectile ions with energy from a few keV to MeV in ion-atom scattering events behave as classical particles because of the de Broglie wave length ranging from 1×10^{-12} to 5×10^{-11} cm short enough more than one order of magnitude compared with the closest approach to a target nucleus. Of course, the He^+ ion scattered from Sr has a higher energy than that scattered from Ti because of the heavier mass of Sr (Sr^{86} : 10 %, Sr^{87} : 7 %, Sr^{88} : 83 %) than that of Ti (Ti^{46} :8 %, Ti^{47} :7 %, Ti^{48} :74 %, Ti^{49} :6 %, Ti^{50} :5 %). A He ion passing through a medium loses its energy gradually via interactions with the electrons in the medium, which in turn gives the information of the depth where the ion undergoes a large angle collision. We employed the semi-empirical formula given by Ziegler[22] for the energy loss, exponentially modified Gaussian profiles as the line shape[23,24], and the Lindhard-Scharff formula to calculate energy straggling values[25].

We measured the MEIS spectra using 120 keV He^+ ions for the as-supplied sample and that annealed at 200, 400, 600, and 800°C in UHV for 30 min, which are shown in Fig. 1. Here, the He^+ ions were incident along the $[11\bar{1}]$ -axis and scattered to 68.3° with respect to surface normal. The vertical arrows indicated in the figure show the energy positions of the scattering components from Ti and Sr atoms on top of the surface. For the as-supplied sample, there is no scattering component from Sr on top, indicating the

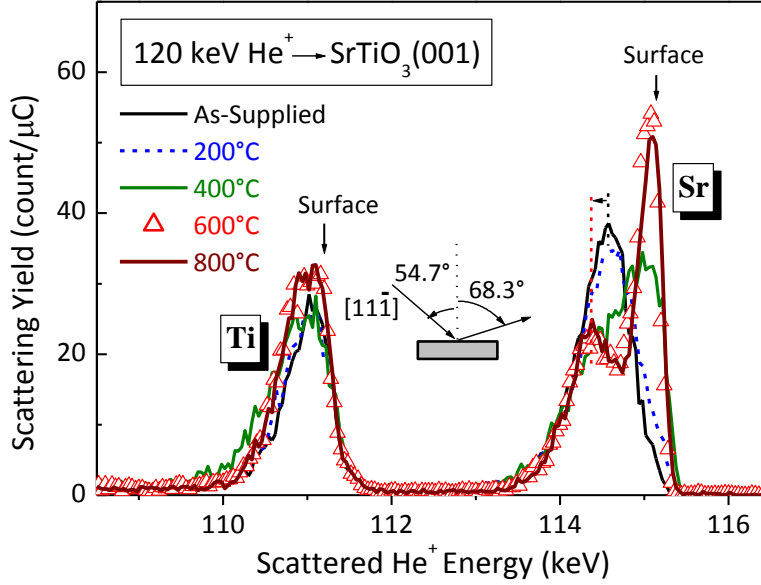


FIG. 1. MEIS spectra observed with 120 keV He^+ ions incident along $[11\bar{1}]$ -axis and scattered to 68.3° with respect to surface normal for as-supplied sample (solid black curve) and that annealed at 200 (dashed blue curve), 400 (solid green curve), 600 (triangles), and 800°C (solid brown curve) for 30 min in UHV. Vertical arrows indicate the energy positions for the He ions scattered from Ti and Sr atoms on top.

surface terminating perfectly with TiO_2 plane. The observed surface peak coming from Ti atoms was well reproduced assuming a SL- TiO_2 termination and the He^+ fraction of 0.5. Note that the as-supplied sample surface even after etching in BHF was contaminated with hydrocarbon about one monolayer (about one monolayer carbon on the surface was confirmed by AES) and the assumed He^+ fraction of 0.5 is close to 0.45 which was determined previously for graphite surface. The observed scattering component from Sr is also fitted well assuming the same He^+ fraction and the $P_{CL}^{(Sr)}(2)$ value of 0.57, indicating significant reconstruction of the contaminated SL- $\text{TiO}_2(001)$ surface, because the $P_{CL}^{(Sr)}(2)$ value is expected to be ~ 0.1 for the bulk truncated surface. The scattering component from Sr on top started to emerge at a temperature of 200°C and a binary peak appeared above 400°C. With increasing annealing temperature, the scattering component from Sr atoms on top was increased, while the 2nd-peak became smaller and shifted to lower energy side. The scattering component from Ti on top of the surface was broadened and increased significantly by annealing. We found no difference between the MEIS spectra observed for the samples annealed at 600 and 800°C. Importantly, the energy position of the 2nd-Sr peak is significantly smaller than that of the Sr peak for the

as-supplied sample. The amount of the Sr segregated on top of the surface is estimated to be 36 % (areal occupation: growth of SrO(001) was assumed). Such MEIS spectrum change clearly indicates that a subsurface atomic re-arrangement took place probably at step edges which are energetically unstable compared with the terraces and then proceeded in a wide range. The situation mentioned above is consistent with that reported by Ohnishi et al.[11]. We then re-etched the surface in hot water (55°C) for 10 min and measured MEIS spectra again. Figure 2 shows the MEIS spectra for the re-etched and that annealed at 200, 400, and 600°C. The MEIS spectrum features are basically almost the same as those for the as-supplied surface except for the fact that the energy position of the Sr-2nd peak coincides with that of the Sr peak before annealing. The difference between the as-supplied and re-etched samples before annealing corresponds to the surface terminated with SL-TiO₂(001) (as-supplied) and DL-TiO₂(001) (re-etched). The present results are inconsistent with the report by Ohnishi et al.[11] that claimed thermal stability of the re-etched surface up to 700°C. This discrepancy possibly comes from different step structure and annealing time.

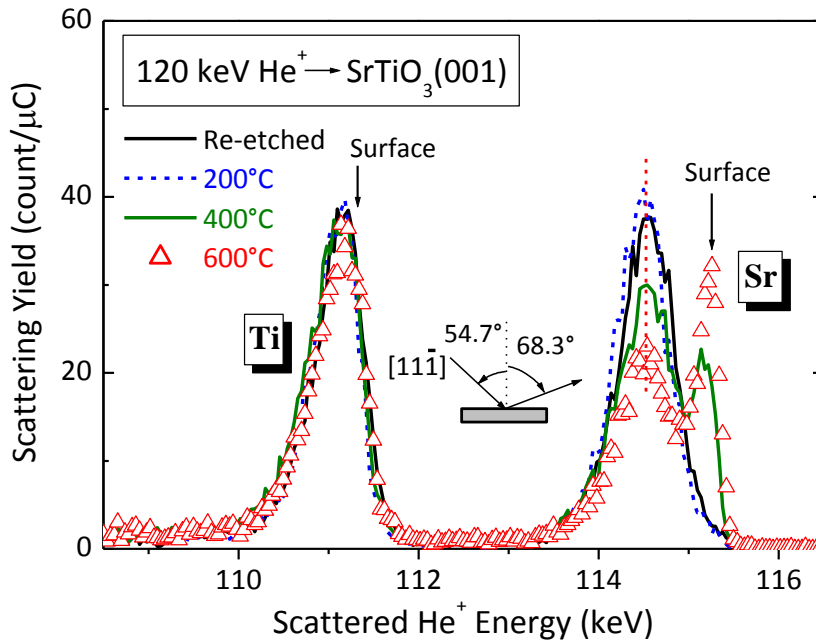


FIG. 2. MEIS spectra observed with 120 keV He⁺ ions incident along $[11\bar{1}]$ -axis and scattered to 68.3° for re-etched (solid black curve) and that annealed at 200 (dashed blue curve), 400 (solid green curve), and 600°C (triangles) for 30 min in UHV.

In order to identify the Sr atoms segregated on top, we observed Sr 3d_{3/2,5/2} lines at incident photon energy of 180 eV under normal emission condition. The photon energy

was calibrated using the 2nd harmonic waves which was incident on a poly crystal Au foil and the work function of the hemispherical energy analyzer was determined to be 3.84 eV assuming that the binding energy (E_B) of Au $4f_{7/2}$ is 84.0 eV scaled from Fermi level. Figures 3(a) and (b) shows the Sr $3d_{3/2,5/2}$ spectra for the as-supplied and re-etched STO, respectively as well as those annealed at 200 (10 min), 400 (10 min), 600, and 800°C in UHV for 30 min. For the as-supplied STO surface, only the Sr $3d_{3/2,5/2}$ lines from STO were observed, whereas the second component with an E_B higher about 1.0 eV

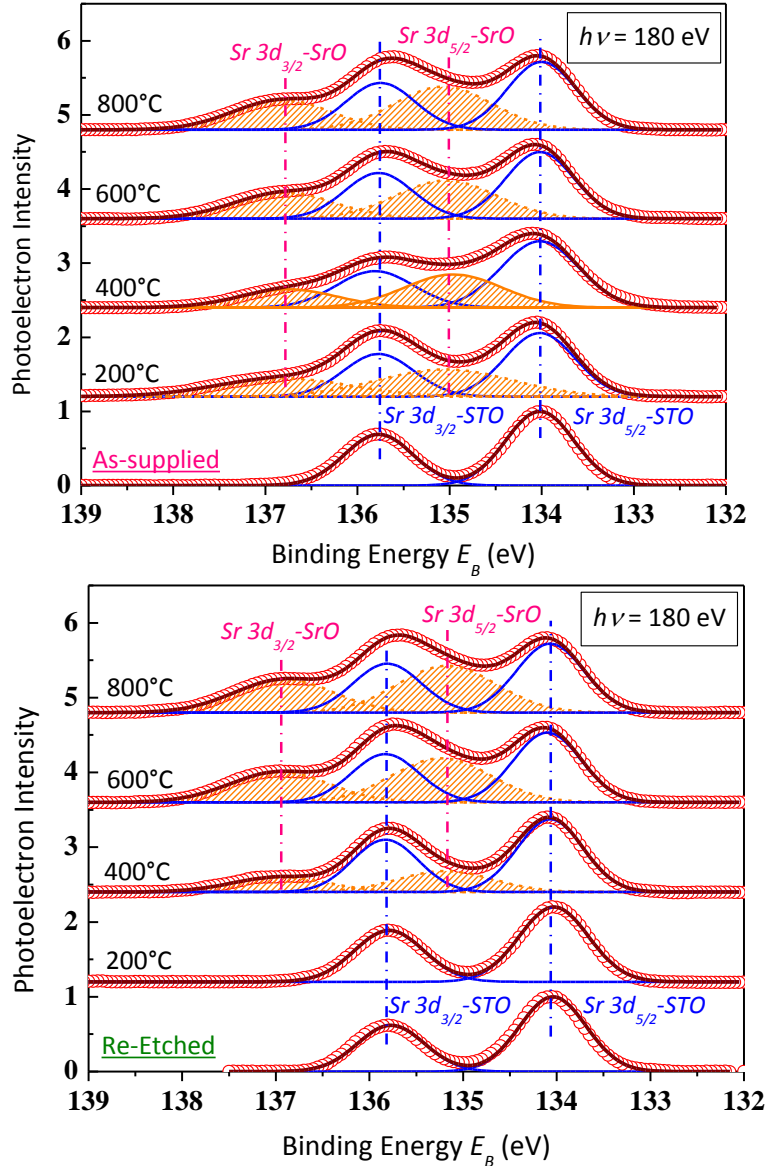


FIG. 3. (a) Sr $3d_{3/2,5/2}$ spectra taken at photon energy of 180 eV for as-supplied sample and that annealed at 200, 400, 600, and 800°C. Observed spectrum was decomposed into two components from STO (blue solid curve) and rock-salt SrO (orange and shaded). (b) Sr $3d_{3/2,5/2}$ spectra taken at photon energy of 180 eV for re-etched sample and that annealed at 200, 400, 600, and 800°C.

than that from STO appeared for the surfaces annealed at temperatures above 200°C for the as-supplied STO and above 400°C for the re-etched STO. This result is well correlated with the previous MEIS observation (see Figs. 1 and 2). Shown in Fig 4 is the Sr 3d spectra observed for the re-etched surface annealed at 400°C under emission angles of 0° (upper) and 60° (lower) scaled from surface normal. The ratio of the intensity for the second component to that for STO increased pronouncedly at emission angle of 60°, indicating clearly the second component corresponds to the Sr segregated on top because of a small escape depth of $\sim 5\text{\AA}$ for the emission energy of $\sim 40\text{ eV}$. According to Kubo et al.[26], there exists Sr adatoms on top of the STO(001) surface annealed at a temperature higher than 900°C in UHV. In this case, however, the E_B of the Sr adatoms should take lower E_B value than that of SrO. Segregation of Sr as oxide clusters was already found by Szot et al.[27] and Kobayashi et al.[12]. The former reported epitaxial growth of SrO whose [100]-axis is parallel to the [110]-axis of STO(001), whereas the latter found crystallized Sr oxide in a disordered form. Considering the higher E_B shift of the Sr 3d line, the second component was identified to rock-salt (RS)-SrO whose Sr-O bond length (2.58 Å) is significantly smaller than that for STO (2.76 Å)[28].

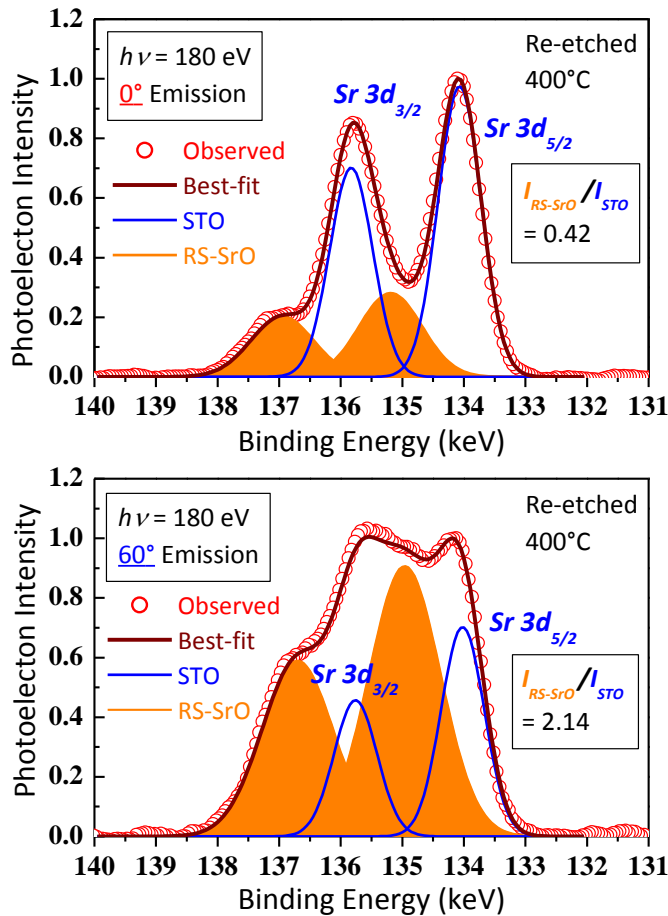


FIG. 4. Sr $3d_{3/2,5/2}$ spectra taken at photon energy of 180 eV for the re-etched sample annealed at 400°C. Emission angle of 0° (upper) and 60° (bottom: surface sensitive) with respect to surface normal. The ratios of intensity for RS-SrO to that for STO are 0.42 at normal emission and 2.14 at emission angle of 60°.

The observed MEIS spectra are well explained by taking account of the formation of RS-SrO clusters on top, which should have at least two atomic-layer (AL) height to be distinguished from the SrO of STO(001). If the height exceeds two ALs, the scattering component from Ti should have a tail on the lower energy side (see Figs. 1 and 2). The fact that the Sr surface peak is very sharp for He⁺ ions incident along the $[11\bar{1}]$ -axis (see Figs. 1 and 2) indicates epitaxial growth of RS-SrO(001) clusters whose $[100]$ -axis is parallel to the $[110]$ -axis of STO(001), as reported by Szot et al.[27]. Indeed, the close encounter probability for the 2nd layer Sr of the RS-SrO(001) is estimated to be ~ 0.25 for the $[11\bar{1}]$ -incidence by the shadowing of the top-layer Sr, resulting in a small contribution to the surface peak. This is the reason why the Sr surface peak is sharp as expected from the system energy resolution and compared with that from Ti. As mentioned before, we determined the He⁺ fraction in advance for He ions emerging from a rutile TiO₂(110) surface to be 0.54 ± 0.02 . For the STO(001) surfaces annealed at 600 and 800°C, the observed surface peak from Ti is reproduced well by assuming DL-TiO₂ termination without shadowing effect on the Ti atoms by overlying RS-SrO(001) clusters because of a large lattice mismatch of 7 % (lattice constant: 3.905 Å for STO and 5.16 Å for RS-SrO). The best-fit was obtained assuming the RS-(SrO)₂ coverage of ~ 20 % for the re-etched surface annealed at 600 and 800°C and simultaneously the He⁺ fraction of 0.55 for the He ions emerging from the DL-TiO₂(001) and RS-SrO(001) surfaces, which coincides well with the value of 0.54 for He ions scattered from the rutile TiO₂(110) surface.

It is an unexpected phenomenon that RS-SrO clusters emerge at low temperatures, even at 200°C for SL-TiO₂ surface and 400°C for DL-TiO₂ termination. Some atomic rearrangement took place probably from step edges, which are reactive and energetically unstable. Based on the density functional theory (DFT), Herger et al.[7] calculated the surface energies for the SL- and DL-TiO₂ terminations and found that the surface energy for the (2×1)-DL-TiO₂(001) termination was quite the same as that for the SL-TiO₂ termination. According to the present MEIS observation, the DL-TiO₂ termination seems significantly stable compared with the SL-TiO₂ surface, although the temperature is limited below 400°C. On the other hand, Ohnishi et al.[11] reported a good thermal stability for the re-etched surface (DL-TiO₂) up to 700°C. According to Heifets et al.[29], the SL-TiO₂ and SrO termination are the most thermally stable rather than the (2×1) reconstructed DL-TiO₂(001) termination under equilibrium condition. However, we must note that annealing in UHV is not the case, because there exist step edges, oxygen

vacancies, and interstitials segregated to the surface, corresponding to a non-equilibrium dynamical process. These discrepancies possibly originate from different conditions of the density of surface defects and subsurface interstitials as well as surface morphology.

B. The Structure of the STO(001)-2×1 Surface

First we check the validity of the two structure models reported so far[6,7] which predicted the DL-TiO₂ terminated 2×1 reconstructed surface. Then the most probable structure model is proposed based on the high-resolution MEIS analysis combined with the *ab initio* calculations. Note that MEIS analysis can check precisely subsurface atomic configurations quantitatively, because Monte Carlo (MC) simulations of the ion trajectories for the given atomic structure make it possible to construct the corresponding MEIS spectrum and to compare it with the observed one. Unfortunately, however, many structure parameters cannot be determined simultaneously like SXRD analysis. Despite that, some relative displacements of the atoms along a major crystal axis can be derived quantitatively using the shadowing and blocking effects[18]. The MC simulations of ion trajectories along the crystal axis considering thermal lattice vibrations give the close encounter probabilities (P_{CL}) for the atoms located in or close to the crystal axis for each atomic layer. Figures 5(a) and (b) show the MEIS spectra simulated assuming the atomic configurations (see Figs. 5(c) and (d)) determined based on the TEM-DFT[6,30] and SXRD-DFT[7,13] analyses, respectively, which are compared with the observed spectrum for 120 keV He⁺ ions incident along the $[11\bar{1}]$ axis and scattered to 68.3° with respect to surface normal. The (2×1) surface was prepared by re-etching in hot water and then annealed at 600°C for 10 min in UHV and the DL-TiO₂ surface was covered partly by RS-SrO(001) clusters with coverage of 22.5 %, which was determined by MEIS. Obviously the spectra simulated assuming both the structure models are far from the observed MEIS spectrum. In the former structure (TEM), the 2nd layer Ti of the DL-TiO₂ shadows the underlying Sr strongly, whereas the latter structure leads to too small shadowing effect. This means that the inter-planar distance between the 2nd-layer Ti and the 3rd-layer Sr is close to that of the bulk SrTiO₃(001) in the former model, while the latter gives too large inter-planar distances than that of the bulk. The other DFT calculations[29] resulted in a structures similar to that determined by TEM analysis[6] and thus the structure also gives a smaller second peak from Sr atoms than the observed one (not shown here).

In order to obtain best-fit spectra, we performed the analysis of *R*-factor defined

below.

$$R \equiv \frac{\sum_i \{ |Y_j^{EXP}(E_i) - Y_j^{SIM}(E_i)| \cdot (Y_j^{EXP}(E_i) / Y_j^{Max}) \}}{\sum_i Y_j^{(EXP)}(E_i)}, \quad (2)$$

where $Y_j^{EXP}(E_i)$ and $Y_j^{SIM}(E_i)$, respectively are observed and simulated scattering yields for He^+ ions scattered from atomic species j with an energy E_i and Y_j^{Max} is the observed maximum yield for He^+ ions scattered from atoms j in the energy range of interest.

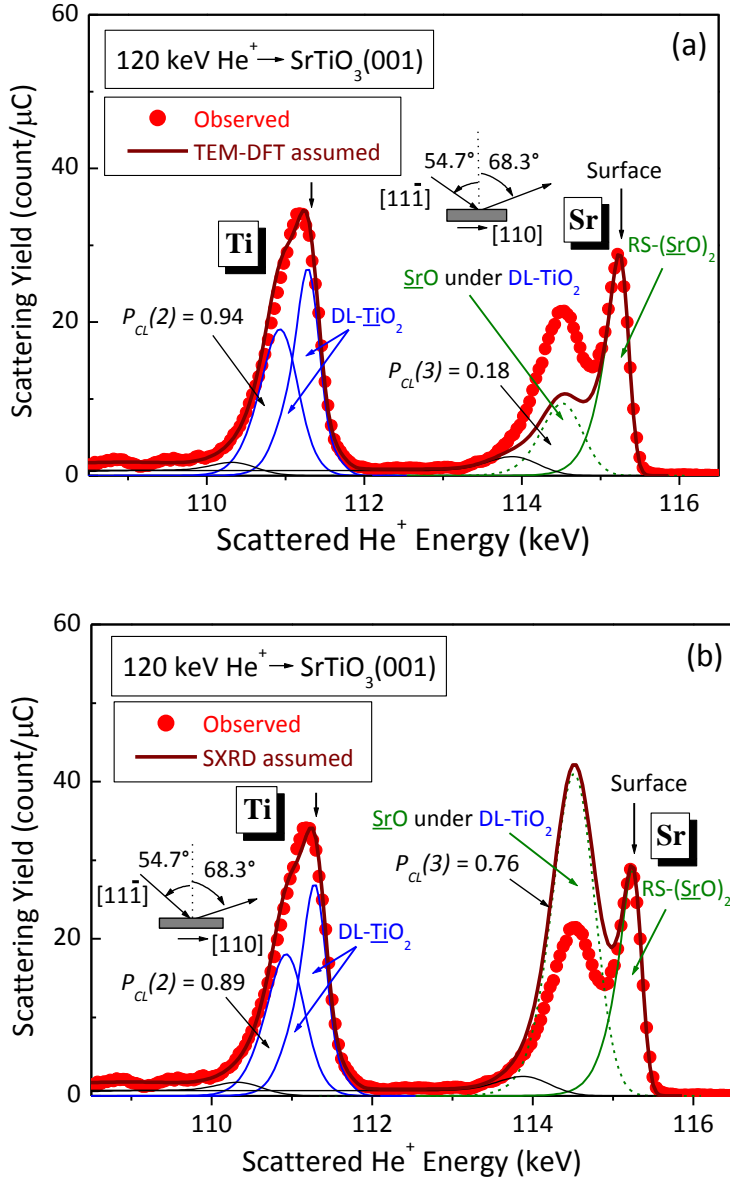
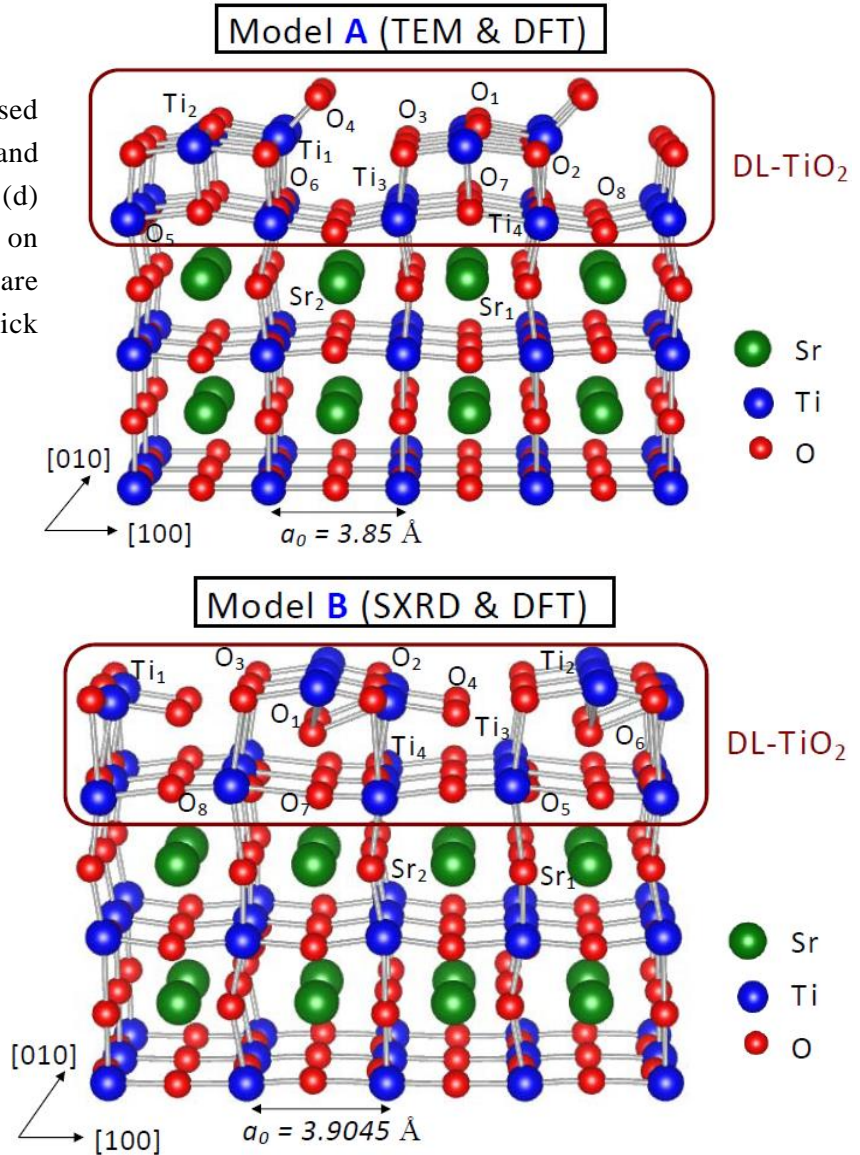


FIG. 5. (a) MEIS spectrum observed with 120 keV He^+ ions incident along $[11\bar{1}]$ -axis and scattered to 68.3° (full red circles) for the substrate re-etched and then annealed at 600°C for 10 min. Thick solid curve (brown) denotes the simulated total spectrum assuming the structure Model A (TEM-DFT). Thin solid and dashed curves (green) correspond to scattering components from RS- SrO and 3rd-layer SrO beneath DL- TiO_2 , respectively. Thin blue curves denote scattering components from Ti of DL- TiO_2 . (b) Observed (full red circles) and simulated (solid and dashed curves) MEIS spectra assuming the Model B (SXR-DFT).

First, we analyze the MEIS spectrum observed for 120 keV He^+ ions incident along the $[11\bar{1}]$ -axis and scattered to 68.3° . Each surface peaks from Ti and Sr are decomposed mainly into two scattering components from the top- and 2nd-layer for Ti and from the

RS-(SrO)₂ and 3rd-layer (beneath DL-TiO₂) for Sr, as shown in Fig. 6. The best-fit was obtained by assuming the RS-(SrO)₂ coverage of 22.5 %, $P_{CL}(2)=0.86$, $P_{CL}(3)=0.38$, and the He⁺ fraction of 0.55 deduced automatically is consistent with the value of 0.54 ± 0.02 observed for TiO₂(110) surface. Both P_{CL} values are intimately related to the surface structure. The slight reduction of $P_{CL}(2)$ for Ti is due to the shadowing by the top-layer O (O₁ and O₄) atoms and the small $P_{CL}(3)$ for Sr is attributed to the shadowing by the 2nd-layer Ti. Figure 7 indicates the top view and side views of two scattering planes at the [110]-azimuth for the DL-(2×1) surface. In this figure, the vertical and lateral displacements of the atoms are ignored for simplicity. Note that there is no displacement along the ×1 direction, which was confirmed by DFT calculations[6,13,29,30]. Under the condition of the [11 $\bar{1}$]-incidence, no significant focusing and blocking effects were observed at this emerging direction (68.3°) within $\pm 2^\circ$.

FIG. 5. (c) Model A proposed based on TEM[6] and DFT[30] analyses and (d) Model B predicted based on SXRD-DFT[7,13], which are depicted by ball and stick model.



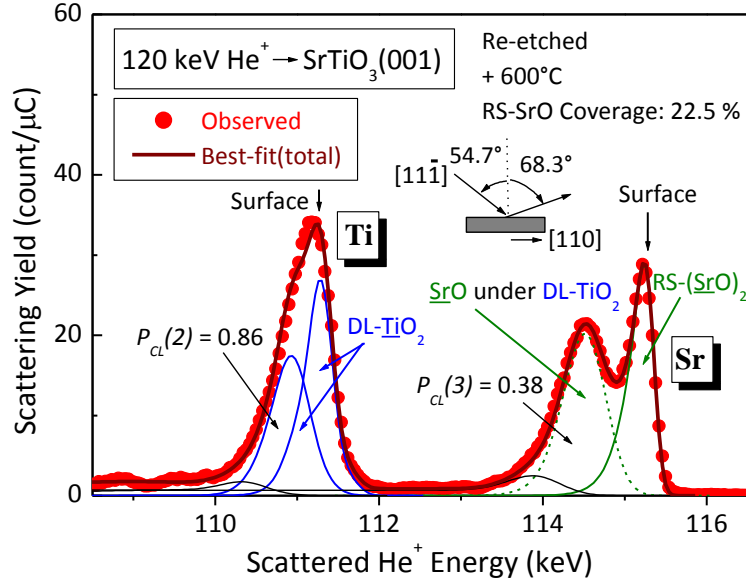


FIG. 6. MEIS spectrum observed for 120 keV He^+ ions incident along $[11\bar{1}]$ -axis and scattered to 68.3° (full red circles) for the substrate re-etched in hot water and then annealed at 600°C for 10 min in UHV. Best-fit (thick solid curve) was obtained assuming $\text{RS}-(\text{SrO})_2$ coverage of 22.5 % on $\text{DL-TiO}_2(001)$, $P_{CL}(2)=0.86$ for Ti atoms in the 2nd-layer of DL-TiO_2 , and $P_{CL}(3)=0.38$ for Sr atoms in the 3rd-layer SrO beneath $\text{DL-TiO}_2(001)$.

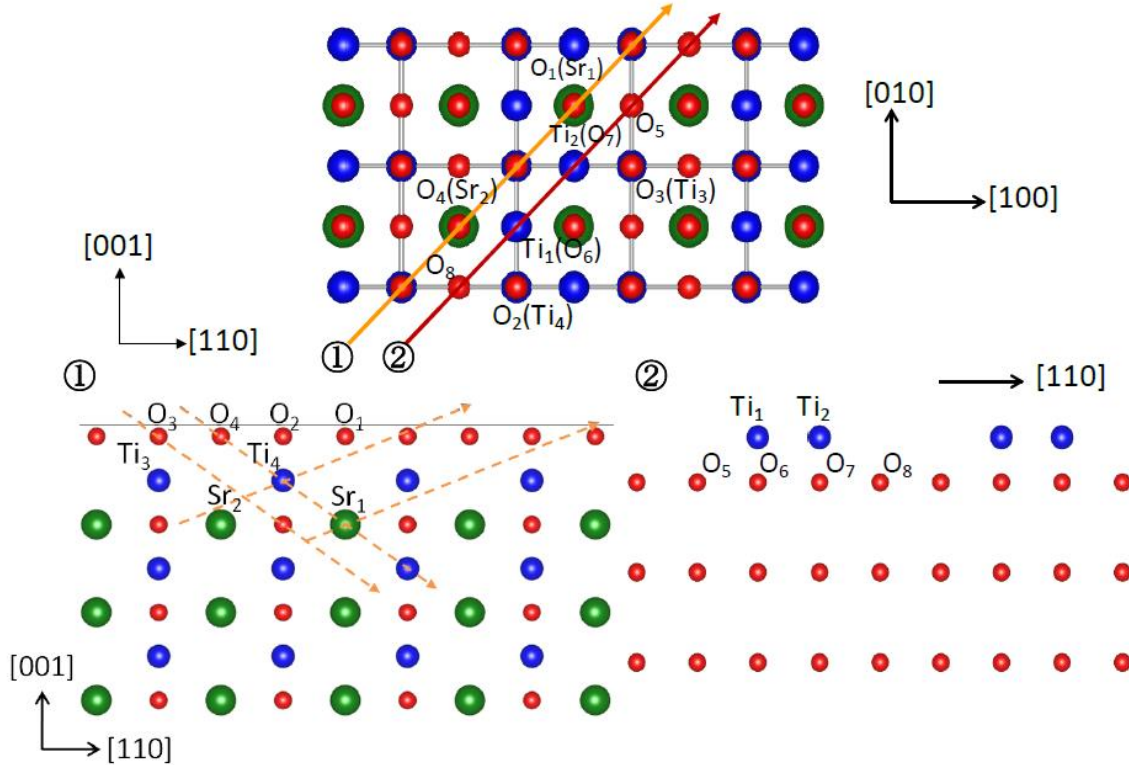


Fig. 7. Top view (upper side) and side views (lower side) of two scattering planes at $[110]$ -azimuth depicted by ball and stick model. For simplicity displacements in x - and z -direction are ignored. Exact displacements of atoms are indicated in Table I.

It is helpful to perform *ab initio* calculations for arriving at the most probable surface structure efficiently. The unit cell consists of the (2×1) periodicity in the (x,y) plane and one DL-TiO₂(001) layer followed by underlying 4×(SrO/TiO₂) layers in the z-direction. The vacuum spacing of 10 Å was inserted between neighboring unit cells in z-direction to avoid interactions between the unit cell slabs. During the simulations, a pair of the last (SrO/TiO₂) layer was fixed. The *ab initio* calculations were carried out using VASP [14,15], in which the generalized gradient approximation (GGA)[31] as the exchange-correlation potentials and projector-augmented wave (PAW) method[32] as the basis functions were employed. We adopted the Residual Minimization/Direct Inversion in the Iterative Subspace (RMM-DIIS) algorithm[15] as an efficient electronic minimization and applied conjugate gradient method[33] to optimize rapidly the configuration of ion cores. The cut-off energy for the plane-wave basis was set to 500 eV. For \vec{k} point sampling to perform fast Fourier transform, 9×7×1 Monkhorst-Pack mesh[34] was used. The calculations were continued until the Hellmann-Feynman force acting on each atom was less than 0.01 eV/Å. As the initial condition, the two atomic models, (A) TEM-DFT[6,30] and (B) SXR[7,13] were assumed. When started from the model (A) structure, it converged rapidly to a slightly changed structure, whereas starting from the model (B) structure needed a very long time to converge and led to the above same structure. The total free energies per unit cell for the model (A) and (B) structures and the optimized structure are -422.35 and -406.55, and -423.84 eV, respectively. The results obtained are compared with the other calculations[13,30]. It is clear that the present result is similar to that predicted based on the TEM-DFT[6,30], although small discrepancies are seen. In contrast, large discrepancies are found between the present data and the SXR-DFT[7,13] model, in particular for the positions of O₁, O₄, O₇, and O₈ as well as the interlayer distance of the DL-TiO₂(001) (see Table I).

In order to reproduce the 2nd surface peak from Sr atoms located on top of the SrO(001) layer beneath the DL-TiO₂(001), we varied the inter-layer distance of the DL-TiO₂(001) (Δ_{I-II}) and that between the 2nd-layer of the DL-TiO₂ and the underlying SrO(001) plane (Δ_{II-III}) without changing any relative atomic positions. Here, the height of each interlayer corresponds to averaged one for two slightly different Ti-planes and Sr-planes for the structure derived from the VASP simulation. The calculated R-factors for each ($\Delta_{I-II}, \Delta_{II-III}$) are indicated as contour-plots in Fig. 8. Here, the R-factors were calculated for the emerging energy range from 110.0 to 112.0 keV for Ti and from 113.6 to 115.5 keV for Sr in the MEIS spectrum. There are two ($\Delta_{I-II}, \Delta_{II-III}$) combinations

minimizing the R -factor; ① (2.323 Å, 1.822 Å) and ② (2.318 Å, 2.082 Å). The top-interlayer distance is almost same but considerable difference is seen for Δ_{II-III} . The calculated total free energy (-423.46 eV) for ② is slightly lower than that (-423.33 eV) for ①. This small difference and slightly larger values about 0.38 - 0.51 eV than that for the optimized structure probably due to small contributions to the total energy from Ti and Sr positive cores.

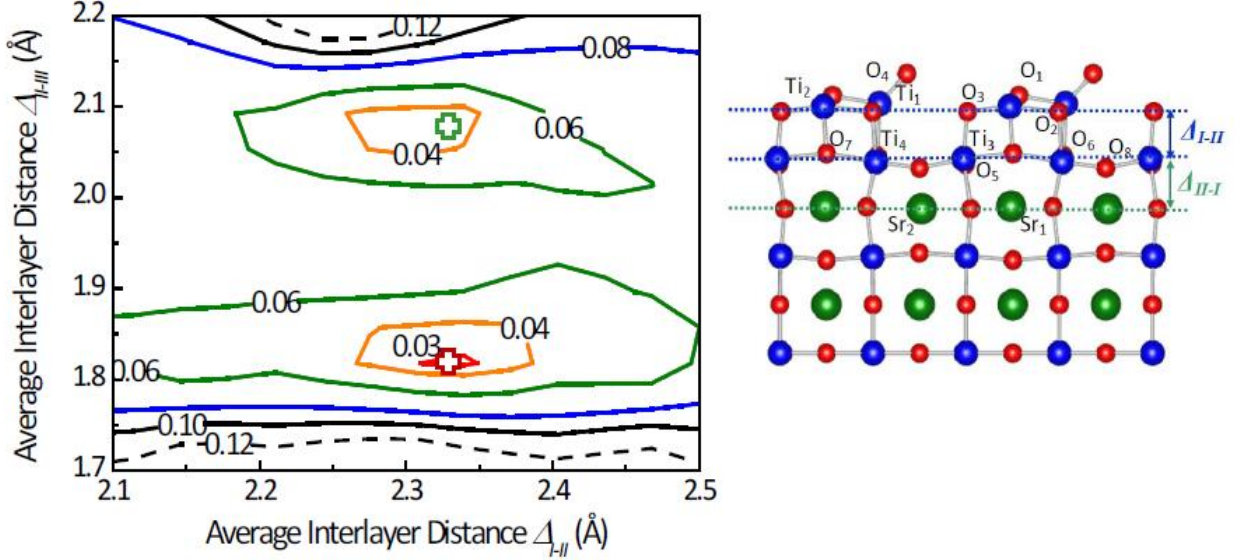


FIG. 8. Contour plot for R -factors calculated for varied interlayer distances, Δ_{I-II} and Δ_{II-III} . Cross symbols indicate the positions minimizing the R -factors.

In order to decide which model corresponds to the most probable structure of STO(001)-2 \times 1 surface, we measured MEIS spectra under different scattering geometries. Figures 9(a) and (b) show the MEIS spectra observed for 120 keV He⁺ ions incident along the $[01\bar{1}]$ -axis and scattered to $[011]$ -direction and to 70° with respect to surface normal. The double-alignment spectrum ($[01\bar{1}]-[011]$) was best-fitted assuming the P_{CL} values of 0.94 ± 0.04 and 0.32 ± 0.04 , respectively for the 2nd- and 4th-layer Ti atoms. Note here that the above values correspond to the squares of the P_{CL} , *i.e.*, $P_{CL}^2(2)=0.94$, $P_{CL}^2(4)=0.32$ due to the approximation that the scattering event happening in the incident path is independent of that in the exit path and time reversibility holds for the emerging path[21]. In this scattering geometry, the 2nd-layer Ti₃ and Ti₄ atoms are not shadowed by the top-layer atoms owing to the large expansion of the top-interlayer distance, while the 4th-layer Ti₅ and Ti₆ are shadowed significantly by the overlying 2nd-layer Ti₃ and Ti₄, respectively, as indicated in Fig.10 (a). This

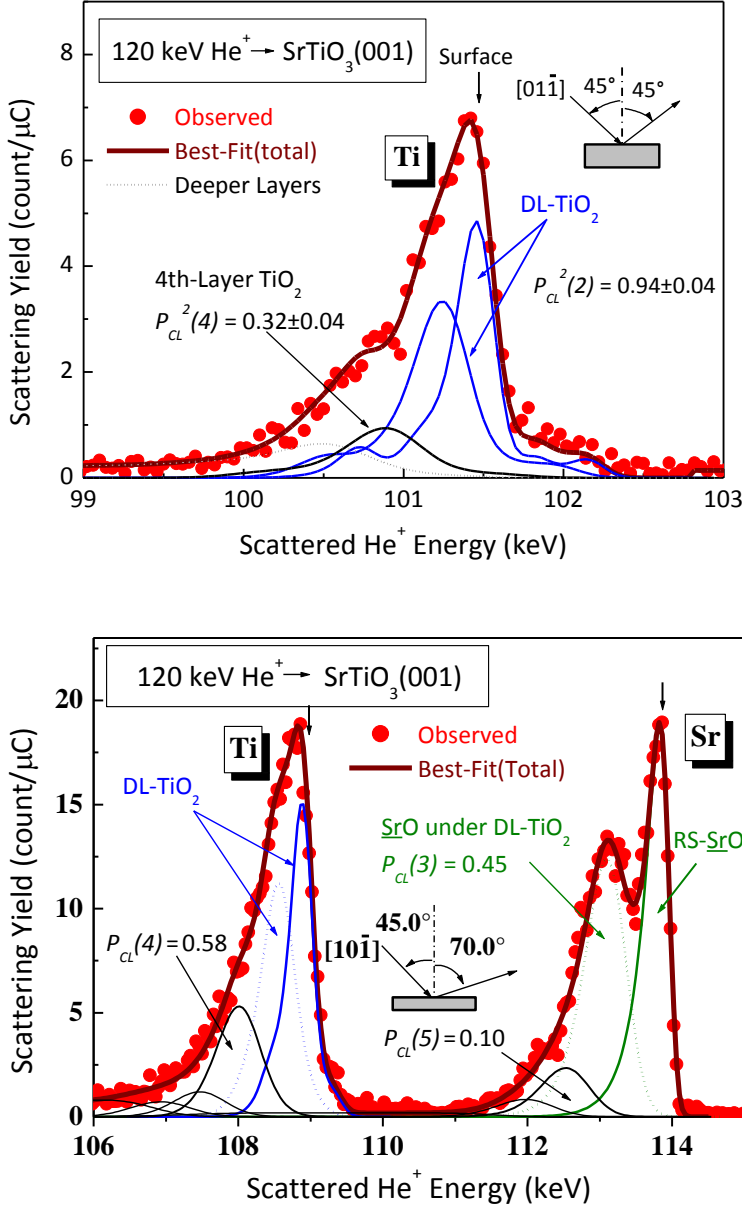


FIG. 9. (Color on line) (a) MEIS spectrum (full red circles) observed with 120 keV He^+ ions incident along the $[01\bar{1}]$ -axis and scattered to $[011]$ -direction from Ti atoms. Solid and dashed curves are best-fitted total (thick solid curve) and decomposed spectra assuming $P_{CL}^2(2) = 0.94 \pm 0.04$ and $P_{CL}^2(4) = 0.32 \pm 0.04$. RS-(SrO)₂ coverage of 25.5 % and He^+ fraction of 0.58 were assumed. (b) MEIS spectrum (full red circles) observed for 120 keV He^+ ions incident along $[01\bar{1}]$ -axis and scattered to 70° at $[010]$ -azimuth. Solid and dotted curves are best-fitted total (thick solid curve) and decomposed spectra assuming $P_{CL}(2) = 1.04 \pm 0.05$, $P_{CL}(3) = 0.45 \pm 0.05$, and $P_{CL}(4) = 0.58 \pm 0.05$.

shadowing depends on the 2nd-interlayer distance. The observed and calculated P_{CL} values assuming the structure models ① and ② are shown in Table II. The observed P_{CL} value for the 4th-layer Ti is nearly equal to that obtained assuming the structure model ②, while significantly larger than that calculated assuming the model ①, although not inconsistent within experimental uncertainties. Here, the uncertainties for the MC simulations mainly come from uncertainties of thermal vibration amplitudes (TVAs). We estimated the root-mean-square TVAs for O, Ti, and Sr to be 0.13, 0.075 and 0.055 Å, respectively from the Debye approximation (Debye temperature: $\theta_D = 402$ K)[35], although the Debye model can be applied only to monatomic materials. Also assumed is enhanced TVAs (the bulk TVAs are multiplied by $\sqrt{2}$) for the top-layer

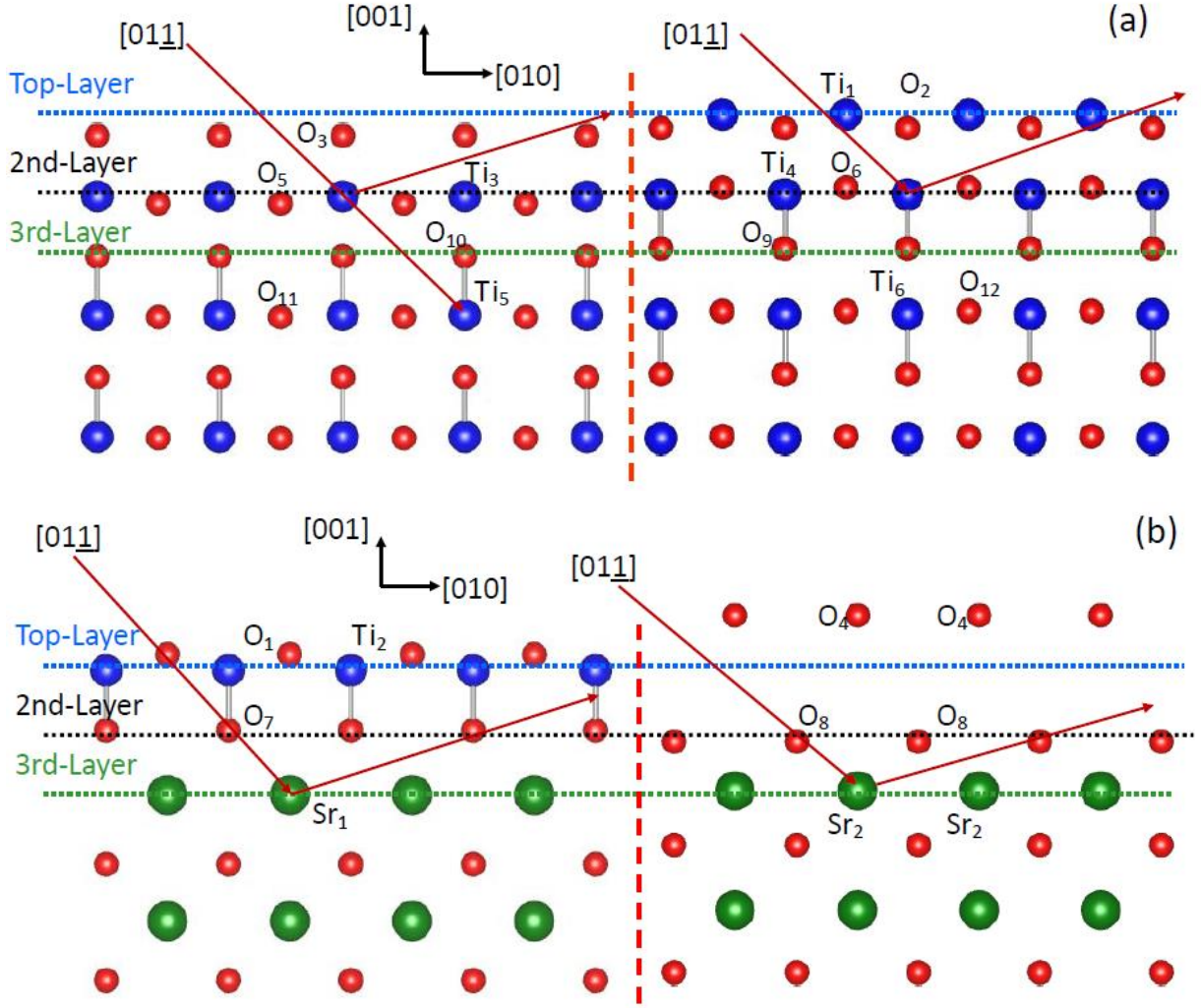


FIG. 10. (a) Side views of two scattering planes consisting of O and Ti at $[010]$ -azimuth and (b) side views of two scattering planes consisting of O, Ti, and Sr at $[010]$ -azimuth.

atoms in the surface normal direction. The MEIS spectrum observed for 120 keV He^+ ions incident along the $[01\bar{1}]$ -axis and scattered to 70° is best-fitted assuming the RS- $(\text{SrO})_2$ coverage of 25.5 %, He^+ fraction of 0.58, $P_{CL}(1)=P_{CL}(2)=1$ for the DL- $\text{TiO}_2(110)$, and $P_{CL}(4)=0.58$ for the 4th-layer Ti atoms under the 3rd-layer $\text{SrO}(001)$. The situation for Ti atoms is quite similar to that for the double alignment geometry, because no blocking effect is expected in the emerging path (random). For the surface peak from Sr, the best-fit is obtained by assuming $P_{CL}(3)=0.45 \pm 0.05$. This P_{CL} value, however, cannot be reproduced assuming the models ① and ②. As can be seen from Fig. 10(b), such a small P_{CL} value is given by the shadowing and blocking of O_7 upon Sr_1 and of O_8 upon Sr_2 . A small displacement of 0.092 \AA to downward direction for O_7 shadows Sr_1 but no blocking effect works in the case of ①, whereas displacement of

0.098 Å in the upward direction for O₈ shadows Sr₂ and O₇ blocks significantly the ions scattered from Sr₁. The results calculated assuming such small vertical displacements are shown in Table II. We must note again that there are no displacements in the $\times 1$ -direction (y -axis). This vertical displacement of O₈ is likely than that of O₇ because of its vertical freedom (see Fig. 5(b)). There is still a small disagreement between the observed and calculated $P_{CL}(3)$ even though considering the small displacement of O₈. The observed P_{CL} value was possibly reduced slightly via shadowing by the overlying RS-(SrO)₂, which was neglected in the MC simulation because of large lattice mismatch of 7 % between the RS-SrO and STO. Considering the results presented above, we conclude that the model ② assuming the small displacement of O₈ is the most probable surface structure of STO(001)- 2×1 reconstruction.

IV. CONCLUSION

High-resolution MEIS analysis revealed unambiguously that the mechanically cut and then chemically etched STO(001) surface is terminated perfectly with SL-TiO₂(001) and the (2×1)-reconstructed surface formed by annealing in UHV is terminated with DL-TiO₂(001). Annealing the surface in UHV induces atomic rearrangement in the subsurface region probably initiated at step edges, which starts from 200°C for as-supplied substrates (SL-TiO₂) and from 400°C for re-etched surface (DL-TiO₂). After annealing at 400 - 800°C the (2×1) surface emerges, onto which crystalline RS-SrO(001) clusters grow epitaxially with two atomic-layer height and the [100]-axis parallel to the [110]-axis of STO(001). Growth of the RS-SrO was evidenced by appearance of the additional component of the Sr 3d_{3/2,5/5} line with a higher E_B shift of 1.0 eV. The coverage of RS-(SrO)₂ is ~30 % for as-supplied substrates and 20~25 % for re-etched surfaces. The thermal stability STO(001) surface is probably dependent mainly on the density of defects and surface morphology.

We checked the two structure models predicting DL-TiO₂ termination for the (2×1)-surface based on electrons and X-ray diffraction analyses combined with DFT. However, both the structure models could not reproduce the observed MEIS spectra. In order to focus on the most probable surface structure efficiently, we also performed the *ab initio* calculations using VASP. The simulation started from the structure proposed based on the TEM observation converged quickly to a structure changed slightly, whereas starting from that predicted by SXRD converged after long time steps to the same structure quite different from the initial atomic configuration. We varied the

Table-I. Present *ab initio* calculations using VASP compared with other DFT simulations [30,13] based on TEM[6] and SXRD[7]. Lattice constant is 3.9045 Å in the present DFT and SXRD-DFT simulations and 3.850 Å in the TEM-DFT calculation.

Atom	Nominal Position	Present DFT		TEM-DFT[30]		SXRD-DFT[13]	
		Δx (Å)	Δz (Å)	Δx (Å)	Δz (Å)	Δx (Å)	Δz (Å)
Ti 1	(1, 1/2, 5/2)	-0.2062	0.4478	-0.2614	0.2728	-0.074	0.757
Ti 2	(3/2, 0, 5/2)	0.1601	0.1537	0.1282	0.1587	-0.109	1.347
O 1	(3/2, 1/2, 5/2)	-0.2051	0.6573	-0.2563	0.6031	0.125	-0.098
O 2	(1, 0, 5/2)	0.0112	0.0309	0.0215	-0.0628	0.328	1.015
O 3	(0, 0, 5/2)	-0.0479	-0.0381	-0.0551	-0.0476	0.000	1.039
O 4	(1/2, 1/2, 5/2)	0.8343	1.7888	0.5291	1.4688	-0.020	0.465
Ti 3	(0, 0, 2)	0.1143	0.0362	0.1056	0.0164	0.351	0.574
Ti 4	(1, 0, 2)	-0.1403	-0.0479	-0.1151	-0.0961	0.141	0.250
O 5	(0, 1/2, 2)	0.0304	-0.1929	0.0292	-0.2010	-0.059	0.273
O 6	(1, 1/2, 2)	-0.1594	0.1696	-0.1841	0.1235	0.293	0.535
O 7	(3/2, 0, 2)	0.0044	0.2767	-0.0098	0.2274	-0.141	0.308
O 8	(1/2, 0, 2)	-0.0062	-0.2952	0.0032	-0.3436	0.066	0.496
Sr 1	(3/2, 1/2, 3/2)	0.0263	0.0852	0.0652	0.0530	0.102	0.070
Sr 2	(1/2, 1/2, 3/2)	-0.0871	-0.0366	-0.0804	-0.0481	0.062	0.078
O 9	(1, 0, 3/2)	0.2442	0.0981	0.2568	0.0333	0.390	0.223
O 10	(0, 0, 3/2)	-0.1960	-0.0425	-0.1991	-0.0432	0.047	0.121
Ti 5	(0, 0, 1)	-0.0875	0.0299	-0.0252	0.0114	0.062	0.137
Ti 6	(1, 0, 1)	-0.0469	-0.0312	0.0149	-0.0222	0.043	0.234
O 11	(0, 1/2, 1)	0.0305	-0.0368	0.0085	-0.0325	-0.062	-0.293
O 12	(1, 1/2, 1)	0.0332	0.0715	0.0014	0.0430	0.082	0.059
O 13	(3/2, 0, 1)	0.0142	-0.1560	-0.0040	-0.1579	0.035	-0.039
O 14	(1/2, 0, 1)	0.0406	0.1601	0.0140	0.1249	0.098	-0.035

Table II. Close encounter probabilities (P_{CL}) derived from MEIS spectra observed for 120 keV He⁺ incident along $[01\bar{1}]$ -axis and scattered to $[011]$ -direction and 70°. The observed P_{CL} values are compared with those calculated assuming the structures predicted by VASP and modified VASP considering MEIS results: MEIS-① (downward displacement of 0.092 Å for O₇) & MEIS-② (upward displacement of 0.098 Å for O₈). For the double alignment geometry the values indicated correspond to $P_{CL}^2(2)$ and $P_{CL}^2(4)$.

	VASP	MEIS-①	MEIS-②
Δ_{I-II}	2.258 Å	2.323 Å	2.328 Å
Δ_{II-III}	1.922 Å	1.822 Å	2.082 Å

Target Atom	Observed P_{CL}^2 [01 $\bar{1}$]-[011]	VASP P_{CL}^2	Simulation P_{CL}^2 MEIS-①	Simulation P_{CL}^2 MEIS-②
2nd-Layer Ti	0.94±0.04	1.0±0.05	1.08±0.05	1.07±0.05
4th-Layer Ti	0.32±0.04	0.18±0.05	0.27±0.05	0.30±0.05
	Observed P_{CL} [01 $\bar{1}$]-70°	VASP P_{CL}	Simulation P_{CL} MEIS-①	Simulation P_{CL} MEIS-②
2nd-Layer Ti	1.04±0.05	0.82±0.07	1.10±0.07	1.10±0.07
3rd-Layer Sr	0.45±0.05	0.76±0.07	0.78±0.07	0.65±0.07
4th-Layer Ti	0.58±0.04	0.39±0.07	0.52±0.07	0.55±0.07

average inter-layer distance of the DL-TiO₂(001) (Δ_{I-II}) and that between the 2nd-layer of the DL-TiO₂ and the underlying SrO(001) plane (Δ_{II-III}) without changing any relative atomic positions. It was found that the combinations ① ($\Delta_{I-II} = 2.323$, $\Delta_{II-III} = 1.822$ Å) and ② ($\Delta_{I-II} = 2.318$, $\Delta_{II-III} = 2.082$ Å) minimized the *R*-factor for the MEIS spectrum observed for 120 keV He⁺ ions incident along the $[11\bar{1}]$ -axis and scattered to 68.3°. In

order to judge which model corresponds to the most probable structure, we also measured under different scattering geometries. As the results, we conclude that the structure model ② accompanying a small upward displacement of 0.098 Å for O₈ is the most probable structure for the STO(001)-2×1 reconstructed surface. This structure is relatively close to that proposed based on the TEM-DFT analysis but considerably different from the structure model predicted by the SXRD-DFT analysis.

ACKNOWLEDGMENTS

The authors would like to thank M. Tagami and N. Takai for their assistance in the MEIS experiments. This work was partly supported by the Ministry of Education, Japan, ‘Academic Frontier Project’.

References

- [1] A.F. Santaner-Syro, O. Copie, T. Kondo, F. Fortuna, S. Pailhès, R. Weht, X.G. Qiu, F. Bertran, A. Nicolaou, A. Taleb-Ibrahimi, P. Le Fèvre, G. Herranz, M. Bibes, N. Reyren, Y. Apertet, P. Lecoeur, A. Barthélémy, M.J. Rozenberg, *Nature* **469**, 189 (2011).
- [2] M. D’Angelo, R. Yukawa, K. Ozawa, S. Yamamoto, T. Hirahara, S. Hasegawa, M.G. Silly, F. Sirotti, I. Matsuda, *Phys. Rev. Lett.* **108**, 116802 (2012).
- [3] Q.D. Jiang, J. Zegenhagen, *Surf. Sci.* **425**, 343 (1999).
- [4] G. Charlton, S. Brennan, C.A. Muryn, R. McGrath, D. Norman, T.S. Turner, G. Thornton, *Surf. Sci.* **457**, L376 (2000).
- [5] M.R. Castell, *Surf. Sci.* **505**, 1 (2002).
- [6] N. Erdman, K.R. Poeppelmeler, M. Asta, O. Warschkow, D.E. Ellis, L.D. Marks, *Nature* **419**, 55 (2002).
- [7] H. Herger, P.R. Willmott, O. Bunk, C.M. Schlepütz, B.D. Patterson, B. Delley, *Phys. Rev. Lett.* **98**, 076102 (2007).
- [8] A. Pancotti, N. Barrett, L.F. Zagonel, G.M. Vanacore, *J. Appl. Phys.* **106**, 034104 (2009).
- [9] M. Kawasaki, K. Takahashi, T. Maeda, R. Tsuchiya, M. Shinohara, O. Ishiyama, T. Yonezawa, M. Yoshimoto, H. Koinuma, *Science* **266**, 1540 (1994).
- [10] T. Nishimura, A. Ikeda, H. Namba, T. Morishita, Y. Kido, *Surf. Sci.* **421**, 273 (1999).
- [11] T. Ohnishi, K. Shibuya, M. Lippmaa, D. Kobayashi, H. Kumigashira, M. Oshima, H.

- Koinuma, Appl. Phys. Lett. **85**, 272 (2004).
- [12] D. Kobayashi, H. Kumigashira, M. Oshima, T. Ohnishi, M. Lippmaa, K. Ono, M. Kawasaki, H. Koinuma, J. Appl. Phys. **96**, 7183 (2004).
- [13] R. Herger, P.R. Willmott, O. Bunk, C.M. Schlepütz, B.D. Patterson, B. Delley, V.L. Shneerson, P.F. Lyman, D.K. Saldin, Phys. Rev. **B 76**, 195435 (2007).
- [14] G. Kresse and J. Hafner, Phys. Rev. **B 47**, 558 (1993).
- [15] G. Kresse and J. Furthmüller, Phys. Rev. **B 54**, 11169 (1996).
- [16] Y. Kido, T. Nishimura, Y. Hoshino, H. Namba, Nucl. Instrum. Methods **B 161-163**, 371 (2000).
- [17] Y. Kido, T. Nishimura, Y. Hoshino, S. Ohtani and R. Souda, Phys. Rev. **B 61**, 1748 (2000).
- [18] R. Courths, B. Cord, H. Saalfeld, Solid State Com. **70**, 1047 (1989).
- [19] Y. Kitsudo, K. Shibuya, T. Nishimura Y. Hoshino, I. Vickridge and Y. Kido, Nucl. Instrum. Methods **B 267**, 56 (2009).
- [20] U. Diebold, Surf. Sci. Rep. **48**, 53(2003).
- [21] J.F. van der Veen, Surf. Sci. Rep. **5**, 199 (1985).
- [22] J.F. Ziegler, J.P. Biersack and W. Littmark, *The Stopping and Range of Ions in Matter* (Pergamon, New York, 1985).
- [23] P.L. Grande, A. Hentz, R.P. Pezzi, I.J.R. Baumvol, and G. Schiwietz, Nucl. Instrum. Methods **B 256**, 92 (2007).
- [24] M. Hazama, Y. Kitsudo, T. Nishimura, Y. Hoshino, P.L. Grande, G. Schiwietz and Y. Kido, Phys. Rev. **B 78**, 193402 (2008).
- [25] J. Lindhard and M. Scharff, K. Dan. Vidensk. Selsk. Mat. Fys. Medd. **27**, 15 (1953).
- [26] T. Kubo, H. Orita, and H. Nozoe, Phys. Chem. Chem. Phys. **13**, 16516 (2011).
- [27] K. Szot, W. Speier, U. Breuer, R. Meyer, J. Szade, and R. Waser, Surf. Sci. **460**, 112 (2000).
- [28] T. Tsuchiya and K. Kawamura, J. Chem. Phys. **114**, 10086 (2001).
- [29] E. Heifets, S. Piskunov, E.A. Kotomin, Y.F. Zhukovskii, D.E. Ellis, Phys. Rev. **B 75**, 115417 (2007).
- [30] K. Johnston, M.R. Castell, A.T. Paxton, M.W. Finnis, Phys. Rev. **B 70**, 085415 (2004).
- [31] J.P. Perdew, K. Burke and M. Ernzerhof, Phys. Rev. Lett. **77**, 3865 (1996).
- [32] P.E. Blöchl, Phys. Rev. **B 50**, 17953 (1994).

- [33] D.M. Bylander, L. Kleinman, and S. Lee, Phys. Rev. **B 42**, 1394 (1990).
- [34] H.J. Monkhorst and J.D. Pack, Phys. Rev. **B 13**, 5188 (1976).
- [35] T. Okuda, K. Nakanishi, S. Miyasaka, and Y. Tokura, Phys. Rev. **B 63**, 113104 (2001).